Supplementary data for the article:

Bjelogrlić, S. K.; Todorović, T. R.; Kojić, M.; Senćanski, M.; Nikolić, M.; Višnjevac, A.; Araškov, J.; Miljković, M.; Muller, C. D.; Filipović, N. R. Pd(II) Complexes with N-Heteroaromatic Hydrazone Ligands: Anticancer Activity, in Silico and Experimental Target Identification. *Journal of Inorganic Biochemistry* **2019**, *199*.
https://doi.org/10.1016/j.jinorgbio.2019.110758

Electronic Supplementary Material

Pd(II) complexes with *N*-heteroaromatic hydrazone ligands: anticancer activity, *in silico* and experimental target identification

Snežana K. Bjelogrlić[a,b], Tamara R. Todorović[c], Milan Kojić[d], Milan Senćanski[e], Milan Nikolić[c], Aleksandar Višnjevac[f], Jovana Araškov[c], Marija Miljković[d], Christian D. Muller[b], Nenad R. Filipović[g,*]

[a] *National Cancer Research Center of Serbia, Pasterova 14, 11000 Belgrade, Serbia*
[b] *Institut Pluridisciplinaire Hubert Curien, UMR 7178 CNRS Université de Strasbourg, 67401 Illkirch, France*
[c] *University of Belgrade - Faculty of Chemistry, Studentski trg 12-16, 11000 Belgrade, Serbia*
[d] *Institute of Molecular Genetics and Genetic Engineering, University of Belgrade, V. Stepe 444a, P.O. Box 23, 11010 Belgrade, Serbia*
[e] *Center for Multidisciplinary Research, Institute of Nuclear Sciences "Vinča", University of Belgrade, 11000 Belgrade, Serbia*
[f] *Physical Chemistry Division, Ruđer Bošković Institute, Bijenička c. 54, HR-10000 Zagreb, Croatia*
[g] *Faculty of Agriculture, University of Belgrade, Nemanjina 6, 11000 Belgrade, Serbia*

*** Corresponding author**

dr Nenad R. Filipović, Associate Professor

Faculty of Agriculture, University of Belgrade
Nemanjina 6, 11000 Belgrade, Serbia
E-mail: nenadf.chem@gmail.com; nenadf@agrif.bg.ac.rs

Experimental part

Anticancer experiments

Cell cultures

Human mammary adenocarcinoma (MCF-7, ATCC® HTB-22) cell line was maintained in DMEM high glucose medium (Dominique Dutscher, Cat No L0102-500), while human acute monocytic leukemia cell line (THP-1, ATCC® TIB-202) was maintained in RPMI-1640 (Life Technologies, Cat. No. 11875-093), supplemented with 10% (v/v) heat inactivated fetal bovine serum (FBS, Life Technologies, Cat No 10270-106) and 1% (v/v) penicillin-streptomycin (10 000 units/mL and 10 000 µg/mL, Life Technologies, Cat No 15140-122). Cells were kept at 37 °C in humidified atmosphere containing 5 % (v/v) CO_2 during their exponential growing phase and in the course of incubation with investigated compounds.

Investigated compounds were initially dissolved in DMSO to the stock concentration of 20 mM. Further dilutions have been performed with RPMI-1640 or DMEM complete media immediately before each experiment, thus the final concentration of DMSO on cells treated with the highest applied concentration of investigated compound was 0.5% (v/v). Cisplatin was dissolved in phosphate buffer solution (PBS) while its further dilutions have been made in DMEM.

Annexin V and propidium iodide (PI) staining

Cells were seeded in 96 flat bottom well plates (Corning® Costar®, Cat. No. CLS3596) in 0.1 mL volume, at density of 10 000 cells/well. MCF-7 cells were left overnight to settle, while treatment of THP-1 cells started 2 h after seeding. Investigated compounds were added in a range of six concentrations. Cells treated with 0.5 % DMSO and cells treated with Celastrol (Enzo Life Sciences, Cat. No. ALX-350-332-M025) at 50 µM were used as negative and positive controls, respectively.

After 24 h of incubation, supernatant medium with non-adherent cells was removed from wells with MCF-7 cells and placed into another 96 well plate. Fresh phosphate buffer saline (PBS) was added to remaining adherent cells afterwards the plate was centrifuged at 450 g for 10 min. Supernatant was discarded and 200 µL of trypsin-EDTA (BioWest, Nuaille, Cat No L0930-100) was added to each well. Cells were detached in about 15 min of incubation at 37 ^{0}C. Trypsin-EDTA was removed after additional spinning cycle, afterwards previously removed supernatants with non-adherent cells were turned back to trypsinized cells. Such prepared samples were stained with Annexin V-FITC (Immuno Tools, Cat No 31490013) and propidium iodide (PI, Miltenyl Biotec IncCat No 130-093-233) each in a volume of 3 µl. Here described trypsinization protocol was applied every time MCF-7 cells were prepared for flow cytometry

analyses, unless is stated otherwise. In case of THP-1 cells, Annexin V-FITC and PI were added on cells right after the incubation time was over.

Plates were analyzed on Guava® easyCyte 12HT Benchtop flow microcapillary cytometer (Millipore, Merck, Darmstadt, Germany) using the dedicated InCyte® software package. Cells were classified according to Annexin V-FITC (green fluorescence) and PI (red fluorescence) labeling on viable (double negative), pre-apoptotic cells (Annexin V-FITC single-stained cells), necrotic cells (PI single-stained cells), and cells in advanced phases of cell death (double-stained cells).

Calculation of $ApoC_{50}$/ $ApoC_{25}$ concentration

Percentages of Annexin V single-stained and double-stained cells were summarized for each concentration of investigated compound and plotted against corresponding concentration. Concentration-response curve was determined using the sigmoidal asymmetric five-parameter logistic equation (GraphPad Prism 6 software). The $ApoC_{50}$ or $ApoC_{25}$ concentrations were computed as those that correspond to 50 % and 25 % of apoptotic events on concentration-response curve, respectively.

Cell cycle analysis

Distribution of cells within phases of mitotic division has been evaluated on remaining cells after Annexin V/PI analysis. Cells were fixed in 70 % ethanol right after the read out of apoptosis assay was finished, and left overnight at 4 °C. Before reading, plates were centrifuged on 450 g for 10 min, ethanol was discarded and PBS added in a volume of 100 µL per well. Cells were stained with 50 µL of FxCycle™ PI/RNAse Staining solution (Molecular Probes, Cat. No. F10797), and incubated at 37 °C for 30 min. Plates were analyzed on Guava® easyCyte 12HT Benchtop flow microcapillary cytometer using the dedicated InCyte® software package.

Inhibition of caspase activity

Cells were treated with investigated compounds at their $ApoC_{50}$ or $ApoC_{25}$ concentrations for 6 h with or without pan-caspase inhibitor carbobenzoxy-valyl-alanyl-aspartyl-[O-methyl]-fluoro methylketone (Z-VAD-fmk, Promega, Madison, USA, Cat. No. G7232). Z-VAD-fmk was added in a concentration that was previously tested and confirmed as non-toxic to cells over 6 h incubation (10 µM for THP-1 cells, and 20 µM for MCF-7 cells). As controls, non-treated cells, cells treated with Z-VAD-fmk only, and cells treated with $ApoC_{50}$/$ApoC_{25}$ concentration only were used. After incubation period was ended, treated cells were carried out for Annexin V/PI staining as described above, and analyzed on Guava® easyCyte 12HT Benchtop flow microcapillary cytometer using the dedicated InCyte® software package. The percent of cell deaths inhibited by Z-VAD-fmk co-treatment was determined using equation:

Inhibition (%) = [1 – (% of apoptosis/necrosis in *A* / % of apoptosis/necrosis in *B*)] × 100

where *A* is the sample treated with Z-VAD-fmk and investigated compound at its $ApoC_{50}$/$ApoC_{25}$ concentration, while *B* is the corresponding sample treated only with the same investigated compound at $ApoC_{50}$/$ApoC_{25}$ concentration.

Caspase-8 and caspase-9 activities

Cells were treated with investigated compound at $ApoC_{50}$/$ApoC_{25}$ concentration for 6 h afterwards activity of caspase-8 and -9 were assayed by means of Guava Caspase 9 SR and Caspase 8 FAM kit (EMD Millipore, Cat. No. 4500-0640), following manufacturer's instructions. Cells were analyzed on Guava® easyCyte 12HT Benchtop flow microcapillary cytometer using the dedicated InCyte® software package.

Generation of mitochondrial superoxide radicals

Cells were treated over 6 h with investigated compound added in concentration of 50 μM, and afterwards stained with MitoSox Red (Molecular Probes, Cat. No. M36008) according to the manufacturer's recommendations. Analysis was performed on Guava® easyCyte 12HT Benchtop flow microcapillary cytometer using the dedicated InCyte® software package.

Assessment of changes in mitochondrial transmembrane potential

Cells were treated over 6 h with investigated compound in concentration of 50 μM. After incubation was terminated, cells were stained with FlowCellect™ MitoDamage Kit (Merck Millipore Corporation, Cat. No. FCCH100106) according to the manufacturer's recommendations. Analysis has been performed on Guava® easyCyte 12HT Benchtop flow microcapillary cytometer using the dedicated InCyte® software package.

Growth inhibition of 3D tumor models

Three-dimensional MCF-7 tumor models were made in 96 well plates (Corning, Cat No 4515). Tumors were left to grow for additional four days afterwards investigated compounds were added in concentrations of 100, 10 and 1 μM. Evaluation has been maintained during 8-day incubation period, with media exchanged on the day 4. Changes in the tumor size have been assessed on Celigo® imaging cytometer (Cyntellect, Brooks Life Science Systems) using Celigo software. Growth rates of non-treated and treated spheroids were computed for every other day during 8-day incubation by dividing the area on the day-n with the area on the day 0.

Acute lethality assay

Artemia salina toxicity assay was conducted as described earlier [S1]. DMSO was used as both, initial solvent for Pd(II) complexes and negative control (0.25% v/v), while cisplatin was used as positive control (dissolved in saline). For each concentration of the tested substances two measurements were performed. LC50 was defined as the concentration of a substance that causes

death of 50% nauplii. DMSO was inactive under the applied conditions. (DMSO did not show a lethal effect under the applied concentrations).

Human serum albumin (HSA) binding experiments

HSA (purity ≥97%), warfarin (analytical standard) and ibuprofen (≥98%) were purchased from Sigma-Aldrich (Germany) and used without further purification. Stock solutions of the complexes and warfarin were prepared in 99.9% DMSO. The 20 mM Tris-HCl solution pH 7.4 (buffer) was prepared with Milli-Q water. The exact stock protein concentration in buffer was determined using an extinction coefficient of 35700 M^{-1} cm^{-1} at 280 nm. Stock solutions were further diluted with buffer and final concentration of DMSO in the protein-ligand mixtures did not exceed 0.5% (v/v). All measurements were done in triplicate, and the appropriate blanks corresponding to various ligands in buffer concentration were subtracted to correct the signal background.

UV absorbance spectra were recorded in the range of 250–320 nm at room temperature, on a NanoDrop 2000c spectrophotometer (Thermo Scientific, USA) equipped with 1.0 cm quartz cell. The final ligand (Pd–complexes) concentrations and constant protein concentration were 0, 5, 10, 20, 30, 40 μM and 10 μM, respectively.

Fluorescence measurements were performed on FluoroMax®-4 spectrofluorometer (HORIBA Scientific, Japan) under thermostatic conditions (Peltier temperature-controlled cuvette holder), and the *excitation and emission* band widths were both *5 nm*. After adding the ligand, the system was kept for equilibration for 2 min before recording the fluorescence spectra. The steady-state protein fluorescence spectra were measured in the absence and presence of the various concentrations of Pd-complexes (2, 4, 6, 8, 10, 12, 14 and 16 μM) at 25, 30 or 37 ºC. The final protein concentration was 1 μM, the excitation wavelength was set at 280 nm (excitation of the Trp and Tyr residues), and the emission spectra were read at 290 to 500 nm. Under the same concentration setup, the synchronous fluorescence spectra were recorded at two different scanning intervals: $\Delta\lambda$ =15 nm (Tyr) and $\Delta\lambda$ = 60 nm (Trp), where $\Delta\lambda = \lambda_{EM} - \lambda_{EX}$; λ_{EM} and λ_{EX} are the emission and excitation wavelengths, respectively.

Fluorescence intensities were corrected for inner filter effect using eq. S1 [S2]:

$$F_c = F_0 10^{(A_{EX} + A_{EM})/2} \quad \text{(eq. S1)}$$

where F_0 is measured fluorescence, F_C is corrected fluorescence, A_{EX} and A_{EM} are absorbances of quencher at excitation and emission wavelength (340 nm), respectively.

To elaborate the fluorescence quenching mechanism, the decrease in protein fluorescence intensity at 340 nm was analyzed using the well-known Stern-Volmer (SV) equation:

$$\frac{F_0}{F_C} = 1 + K_{SV}[Q] \quad \text{(eq. S2)}$$

where F_0 and F_C are protein emission fluorescence at 340 nm without and with addition of ligand, respectively, [Q] is total quencher (ligands) concentration, and K_{SV} is SV quenching constant.

The estimation of the association (binding) constant (K_a), and number of binding sites (n) for binding of small molecule to set of equivalent sites on a macromolecule was done using the modified SV equation [S11]:

$$\log\frac{F_0 - F}{F} = -n\log\frac{1}{[L] - [P]\frac{F_0 - F}{F_0}} + n\log K_a \quad \text{(eq. S3)}$$

where [P] and [L] are total concentration of protein (HSA) and ligand (Pd-complexes). The values of n and K_a were obtained from the slope and intercept of the modified SV plot, respectively.

In competition binding experiments, 10 min pre-incubated equimolar mixtures of HSA–warfarin or –ibuprofen (1 μM) were titrated with Pd–complexes up to five-fold molar excess. An excitation wavelength of 280 nm was selected, and fluorescence spectra were recorded in the range of 300–500 nm. Ligands binding constants were calculated as described above.

The circular dichroism (CD) measurements were carried out on Jasco J-815 spectropolarimeter (Japan Spectroscopic, Japan). Far-UV CD spectra of HSA (30 μM) in the presence and absence of ligands (30 μM and 120 μM) were recorded in the range of 200–250 nm at room temperature, under constant nitrogen flush, with an accumulation of three scans. Mean residue ellipticity (MRE) was calculated from equation:

$$\mathbf{MRE} = \frac{\theta}{10\ r\ l\ [HSA]} \quad \text{(eq. S4)}$$

where θ is ellipticity in mdeg at 209 nm, r is number of amino acid residues (585), l is the path length of the cell in cm (0.01), and [HSA] is molar concentration of protein.

The α-helical content of free and bound HSA was calculated from MRE values at 209 nm using the following equation [S3]:

$$\%\ \alpha\text{-helix} = \frac{-MRE_{209\,nm} - 4000}{33000 - 4000} \times 100 \quad \text{(eq. S5)}$$

where MRE_{208} is the observed MRE value at 208 nm, 4000 is the MRE of the β–form and random coil conformation cross at 208 nm and 33,000 is the MRE value of a pure α–helix at 208 nm.

Molecular docking

The crystal structure of HSA in complex with warfarin was downloaded from RCSB database, PDB code 2BXD [S4]. For DNA structures, we chose two, PDB coded 3U2N [S5] and 4U8A [S6]. The crystal structure of topoisomerase I (Top I) in the complex with camptothecin was

downloaded from RCSB database, PDB code 1T8I [S7]. The crystal structure of topoisomerase II (Top II) in the complex with etoplatin was downloaded from RCSB database, PDB code 5GWI [S8]. All heteroatoms from crystal structures were removed, leaving only protein or DNA. Ligands were built in Avogadro and initially geometrically optimized using MMFF94 force field [S9]. They were further optimized on B97D level of theory [S10], using 6-31g++ [S11, S12] basis set for C, N O and H atoms and LanL2DZ [S13–S15] for Pd atom in Gaussian09 D.01 software [S16]. Protein, DNA and ligand structures were prepared in Autodock Tools 1.5.6 [S17, S18]. Partial charges on ligand atoms in were calculated using MOPAC2016 [S19] on PM7 [S20] level of theory with COSMO solvation model in case of Tops I and II docking. Dielectric constant was set to 12.4 (pyridine). The grid box for HSA was set in center of warfarine binding site, with dimensions 40×40×40 and grid spacing 0.375 Å. For docking into DNA structures, the grid box dimensions were 88×88×126. The grid box for Top I was set in the center of receptor camptothecin binding site, with dimensions 60×60×60. The grid box for Top II was set in the centre of receptor etoplatin binding site, with the same dimensions as for Top I. The simulated annealing protocol was used to dock ligands into receptors, with 100 runs and 50 cycles. The Pd parameters were taken from Molecular Graphics Laboratory site (http://mgl.scripps.edu/). Docking was carried out in Autodock 4.2.6 [S18].

Top I Activity Inhibition Assays

Top I reaction was conducted in the reaction mixture (20 µL) containing buffer Tango (33 mM Tris–acetate pH 7.9, 10 mM magnesium acetate, 66 mM potassium acetate, 100 µg mL^{-1} bovine serum albumin (BSA); Thermo Scientific, Waltham, *Massachusetts*, USA), 200 ng of pBlueScript SK (-) plasmid (supercoiled DNA substrate) and **1** or **3** (in DMSO) at the appropriate concentration. After addition of one unit of Top I (Invitrogen, Carlsbad, California, USA) the mixtures were incubated for 30 min at 37°C. The same mixture to which was added only DMSO or DMSO and Top I, but not chemical inhibitors were used as negative and positive control reactions, respectively. The composition of DNA molecules was analyzed by electrophoresis on 0.9% agarose gel (at a constant voltage of 80 V) in 1 × TAE buffer (40 mM Tris, 20 mM acetic acid, 1 mM EDTA). The gel was stained with 1µg mL^{-1} ethidium bromide solution (30 min at room temperature), distained in distilled water (30 min at room temperature) and visualized under UV light.

Gel electrophoresis study of interactions with plasmid DNA

The interaction of **1** and **3** with plasmid DNA was investigated by agarose gel electrophoresis. pBlueScript SK (-) plasmid (0.01 M) in 5 mM Tris buffer (pH = 7.2) was treated with **1** and **3** at 37 °C. The samples were incubated for 90 and 120 min, and then loading buffer was added. The samples were then examined by electrophoresis at 6 V cm^{-1} on 0.9% agarose gel using Tris–boric acid–EDTA buffer. After electrophoresis, the bands were visualized using UV light and photographed. The cleavage reaction was initiated by the addition of the complex and quenched with 2 µL of the loading buffer.

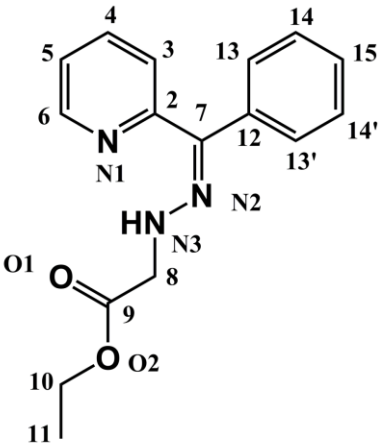

py2bzhaOEt

Scheme S1. Atom numbering used in NMR

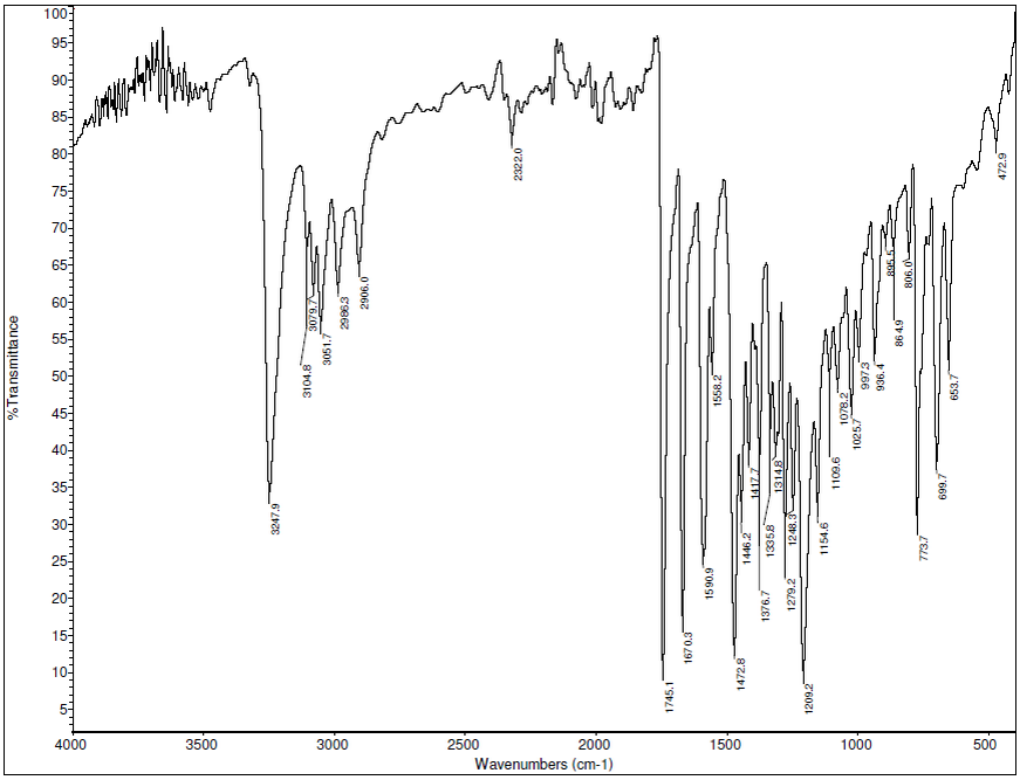

Fig. S1 IR spectrum of **5.**

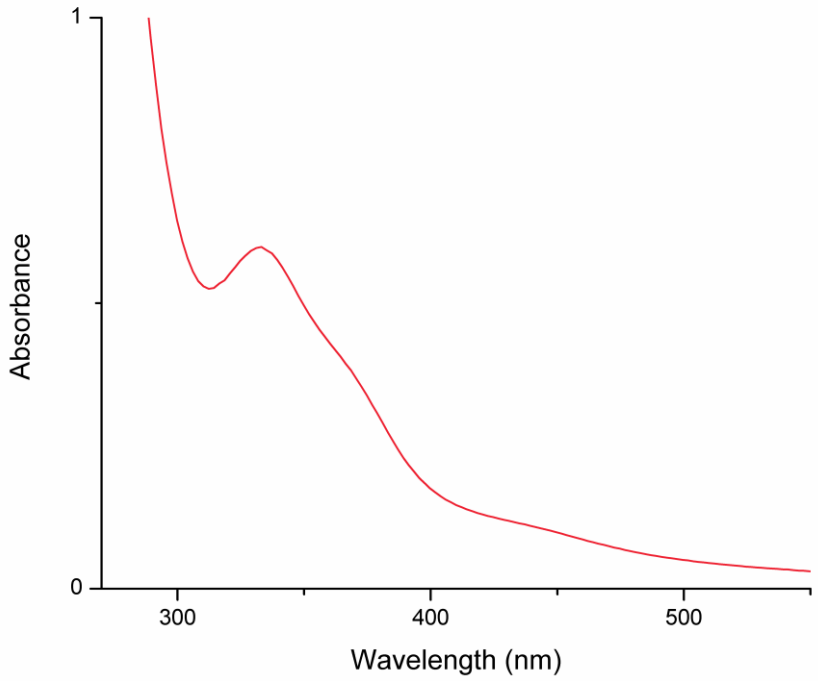

Fig. S2 UV/Vis spectrum of **5** in DMSO.

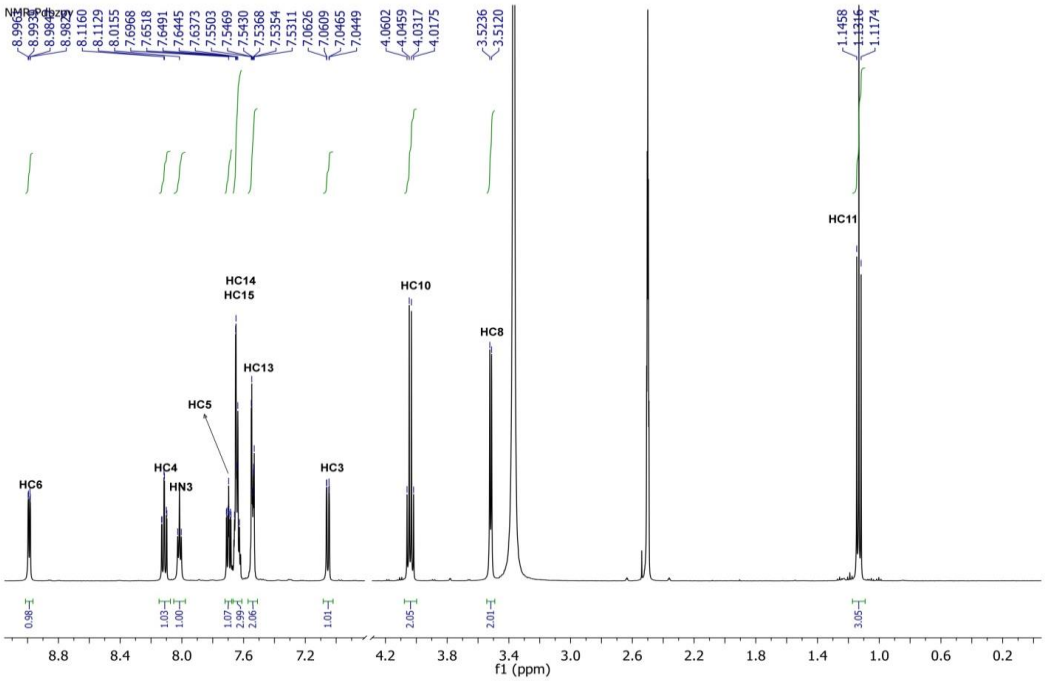

Fig. S3 ^{1}H NMR spectrum of **5** in DMSO-d_6.

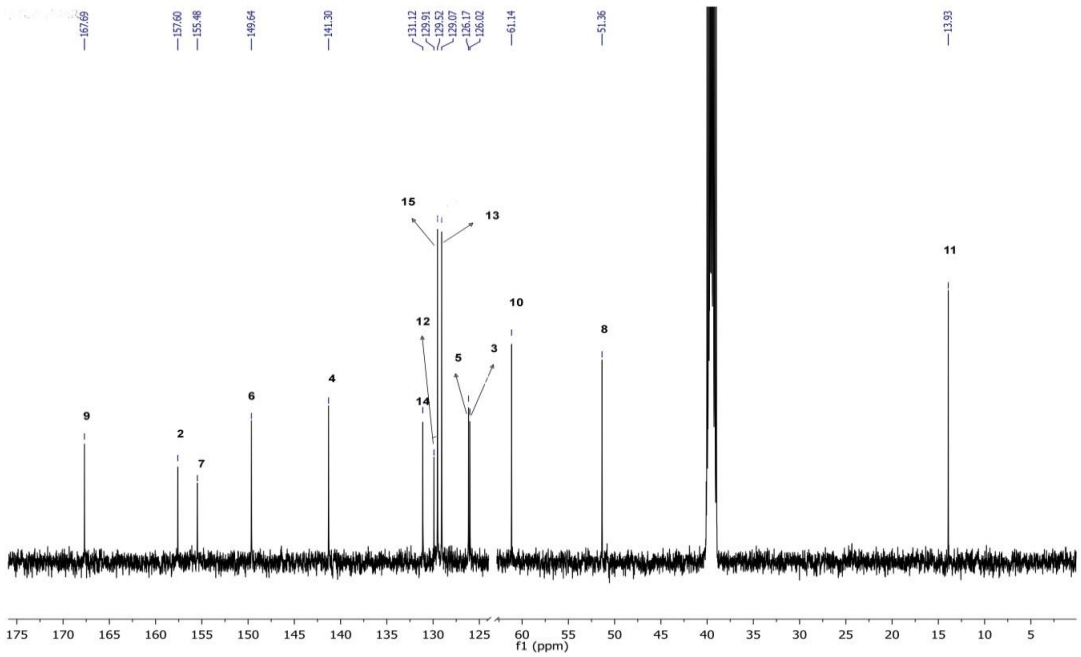

Fig. S4 ^{13}C NMR spectrum of **5** in DMSO-d_6.

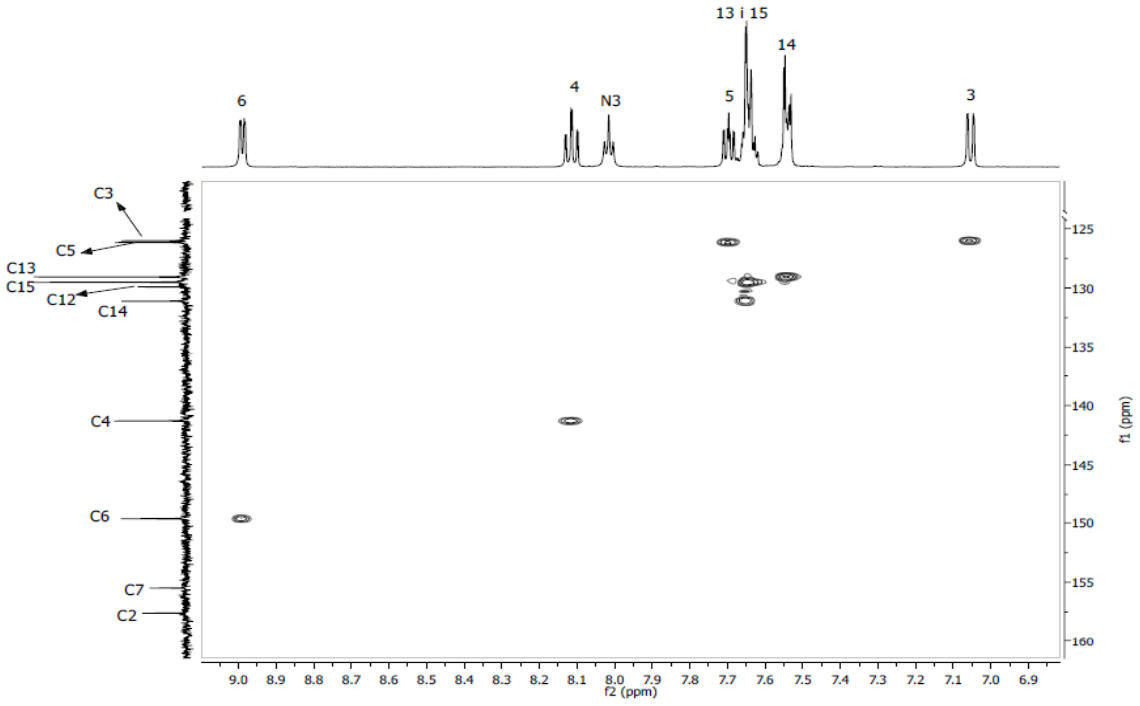

Fig. S5 2D HSQC spectrum of **5** in DMSO-d_6.

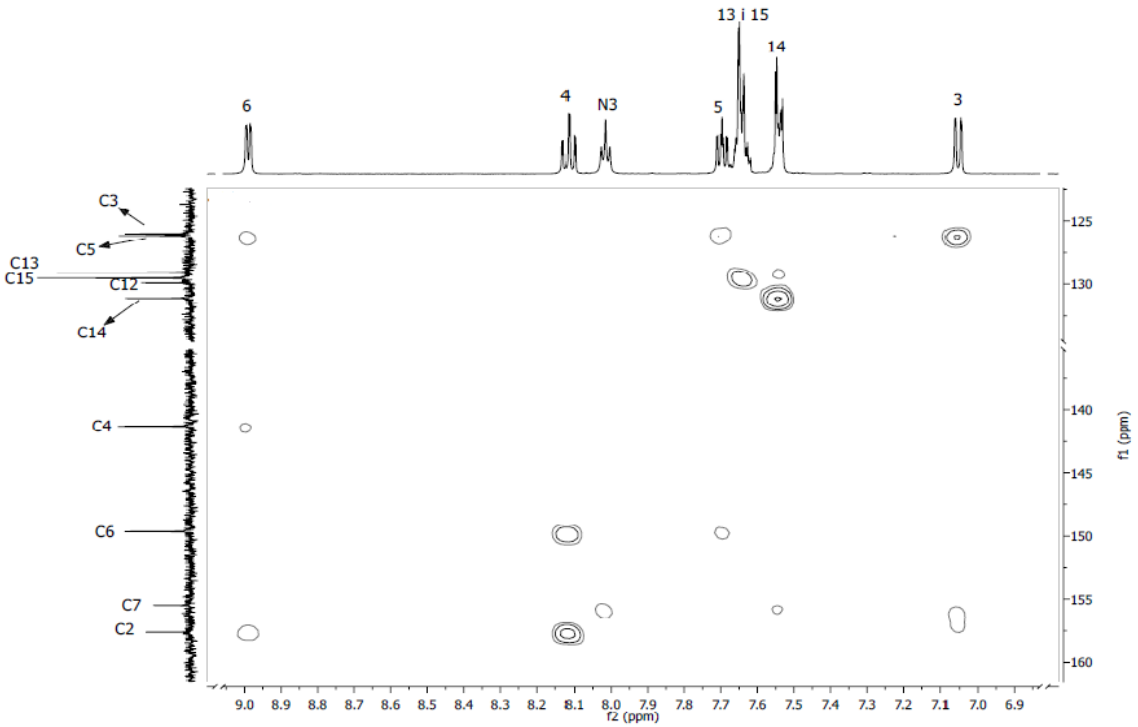

Fig. S6 2D HMBC spectrum of **5** in DMSO-d_6.

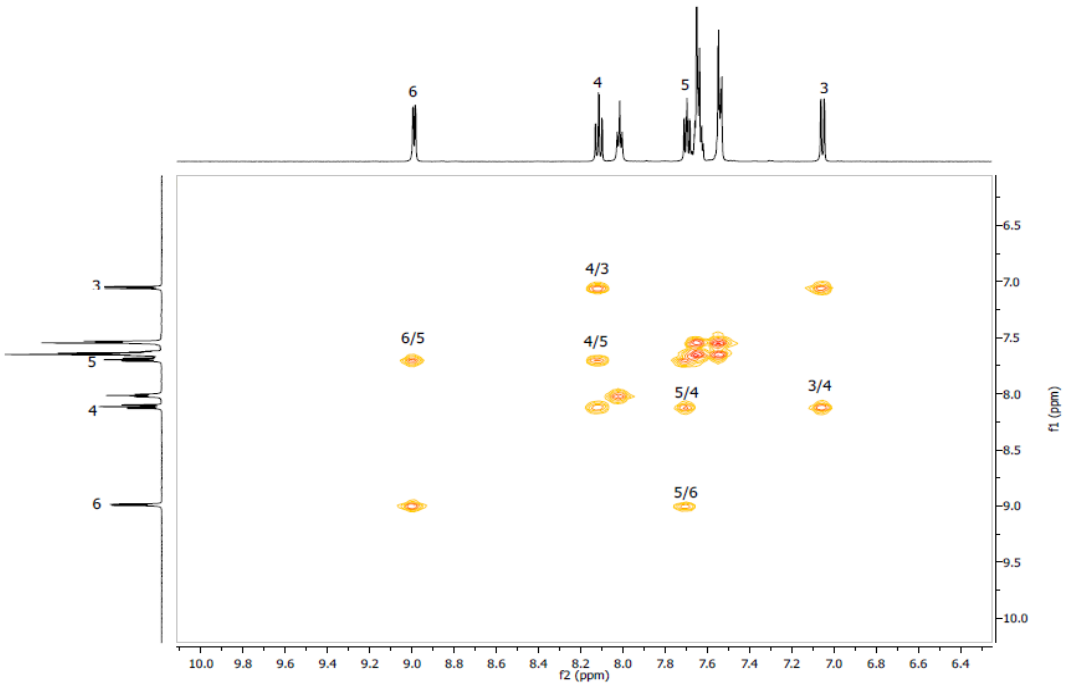

Fig. S7 2D COSY spectrum of **5** in DMSO-d_6.

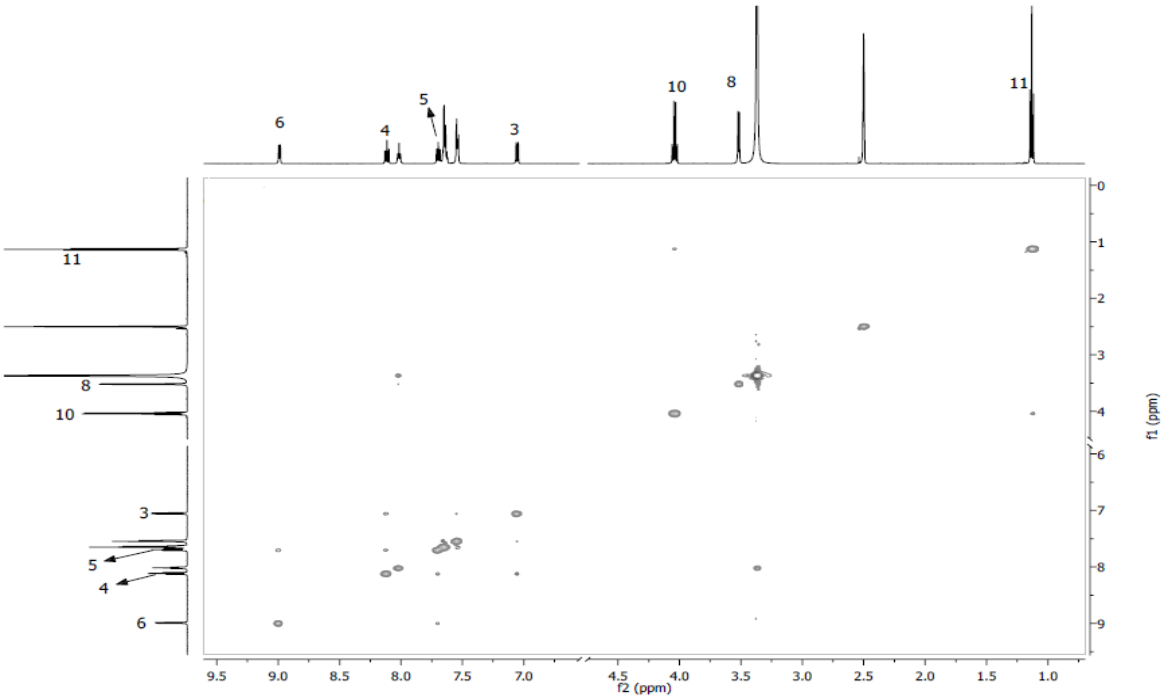

Fig. S8 2D NOESY spectrum of **5** in DMSO-d_6.

Results and discussion

Synthesis and characterization

In our previous work Pd(II) complexes **1**–**4** with ligands q8ahaOEt, q2ahaOEt, py2ahaOEt, and py2achaOEt were obtained by template reactions of $K_2[PdCl_4]$, haOEt×HCl and corresponding *N*-heteroaromatic carbonyl compounds [S21] NN' bidentate mode of coordination for this class of ligands was confirmed in both solution and solid state. In this work, novel Pd(II) complex with *in situ* obtained py2bzhaOEt ligand was synthesized by the same procedure - mixing of ethanolic solution of py2bz and haOEt×HCl with water solution of metal salt (Scheme S2). The results of elemental analysis confirmed that py2bzhaOEt was formed and that the inner sphere of the complex contains two chlorides and one palladium ion per ligand. The value of molar conductivity of **5** in DMSO is significantly lower than threshold value for 1 : 1 electrolytes [S22], pointing to the non-electrolyte nature of the complex. In the IR spectrum of **5** several characteristic vibrations were noticed and assigned: ν(N–H) at 3244 cm^{-1}, ν(C=O) strong band at 1743 cm^{-1}, as well as very strong band at 1205 cm^{-1} which originates from ν(C–O). Also, strong, characteristic band at 1586 cm^{-1} is due to C=N group, while low intensity ν(N–N) vibration was noticed at 1024 cm^{-1}. These values are very close to corresponding data obtained for **1**–**4** [S21]. The presence of the signal at 8.02 ppm, assigned to N3–H, in ^{1}H NMR spectrum of **5** indicates that pybzhaOEt is coordinated to Pd(II) in neutral form. The obtained spectroscopic data corroborate molecular structure of **5**, where the neutral ligand binds the metal in a bidentate fashion, while the remaining two metal coordination sites are occupied by chloride ions. This is also confirmed by single crystal X-ray diffraction.

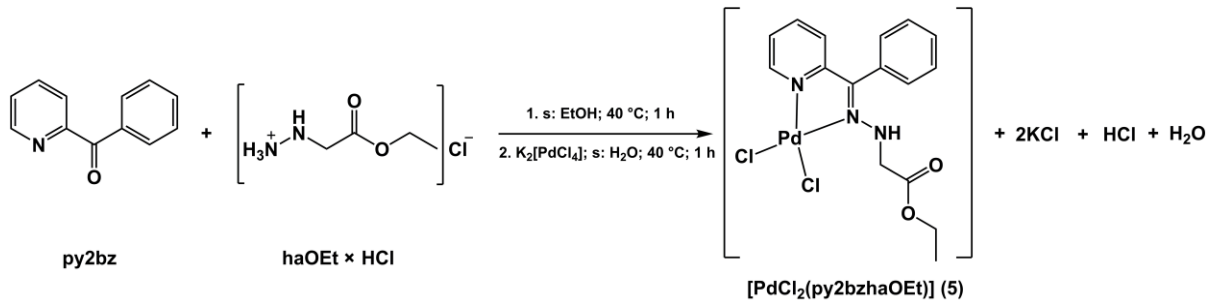

Scheme S2. Synthesis of $[PdCl_2$(py2bzhaOEt)] (**5**)

Table S1 summarizes crystallographic data for **5**. Molecular structure of **5** with the atom numbering is given in Figure S9. Compound **5** is a molecular complex in which palladium ion sits in the center of the slightly distorted square planar coordination environment formed by pyridine nitrogen N1, imine nitrogen N14, and two chloride anions (which balance the metal charge). A descriptor τ for the geometry of the coordination sphere equals to 0.08, which is fairly close to a theoretical value of 0.00 for an ideal square planar coordination core [S23]. Crystal

packing of **5** is characterized by isolated complex molecules with only one bifurcated intramolecular hydrogen bond observed. Table S2 summarizes geometrical details of a single bifurcated H-bond [S24] where the imine nitrogen N15 acts as a double donor towards intramolecular acceptors Cl2 and O1.

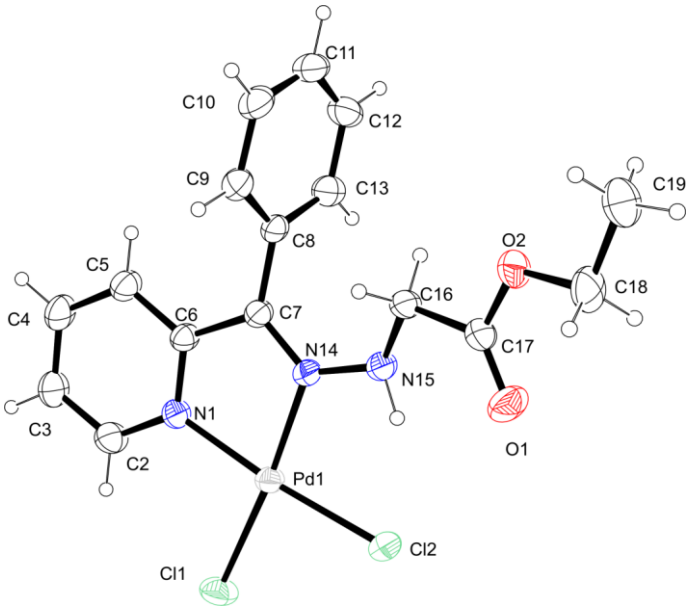

Figure S9. ORTEP drawing of **5** with the atom numbering. Thermal ellipsoids are given at the 50% probability level. Selected bond lengths [Å] and angles [°] with e.s.u.'s in parentheses: Pd–N1, 2.013(3); Pd–N14, 2.026(4); Pd–Cl1, 2.2883(14); Pd–Cl2, 2.2945(12); N1–Pd–N14, 79.52(14); N1–Pd–Cl1, 95.05(9); N1–Pd–Cl2, 174.38(9); N14–Pd–Cl1, 174.52(11); N14–Pd–Cl2, 94.86(11); Cl1–Pd–Cl2, 90.57(5).

Table S1 Crystallographic data for **5**

Structure	**5**
Brutto formula	$C_{16}H_{17}Cl_2N_3O_2Pd$
Formula weight ($gmol^{-1}$)	460.62
Crystal color and habit	Yellow stick
Crystal dimensions (mm)	0.02 x 0.03 x 0.17
Space group	$P2_1/n$
a (Å)	14.4227 (3)
b (Å)	7.2284 (2)
c (Å)	17.7189 (4)
β (°)	101.744 (2)
V ($Å^3$)	1808.58 (8)
Z	8
μ (CuK_α) (mm^{-1})	11.115
Absorption correction	Multi-scan
F(000)	920
θ max (°)	62.29
No. refl. measured	5039
No. refl. unique	2799
No. refl. observed [$I>2\sigma(I)$]	2420
R_{int}	0.0393
R_σ	0.0566
Parameters	222
R_1 [$I>2\sigma(I)$]	0.0389
wR_2, all	0.1019
S	1.002
ρ_{max}, ρ_{min} ($eÅ^{-3}$)	0.75, -0.64

Table S2 H-bond parameters in the structure of **5**

D-H···*A*	H···*A* (Å)	*D*···*A* (Å)	*D*-H···*A* (°)	*D*-H···*A*
N15-H···Cl2	0.92 (5)	2.29 (6)	3.076 (4)	144 (5)
N15-H···O1	0.92 (5)	2.29 (6)	2.706 (6)	103 (4)

Stability of the complexes 1 and 3

The aqueous solution behaviour with respect to hydrolysis of **1** and **3** was studied in DMSO/H_2O 1:100 (v/v) at 298 K over 24 h by UV-Vis spectroscopy. The complexes were relatively stable, as can be seen from their electronic absorption spectra (Figure S10). Complex **1** showed less than 2% decrease of the intensity of the band with an absorption maximum at 333 nm (Figure S10A), while decrease of the intensity of the band at 329 nm for complex **3** was less than 5% (Figure S10B).

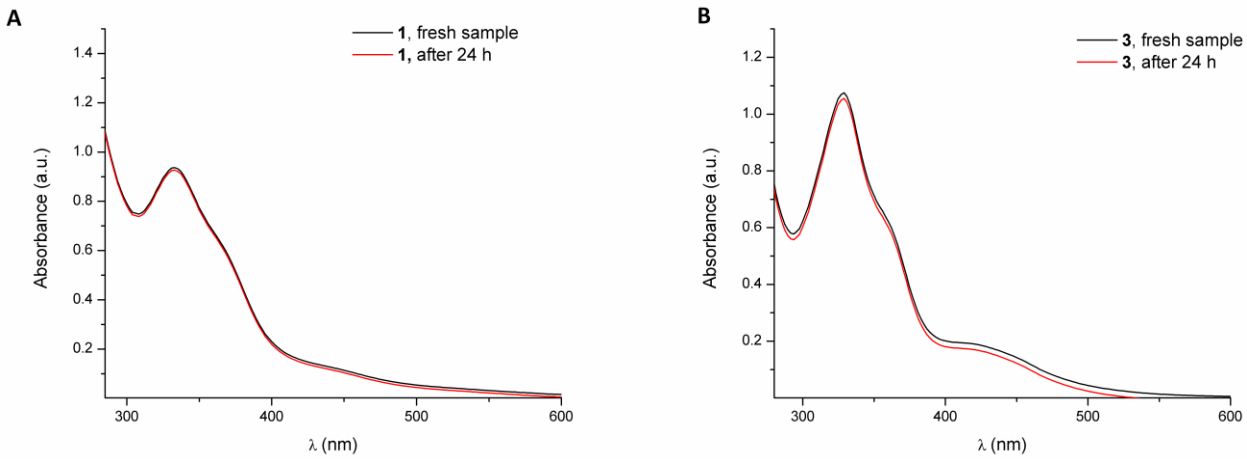

Fig. S10. UV-Vis spectroscopy data of **1** (A) and **3** (B) in DMSO/H_2O 1 : 100. First measurement (black), after 24 h (red).

Molar conductivity measurments of freshly prepared solutions of **1** and **3** in DMSO and conductivity measurments of the same samples after 24 h coborrate stability of the complexes since incerase in Λ_M for both samples after 24 h was less than 2.5 $\Omega^{-1}\,cm^2\,mol^{-1}$.

Anticancer experiments

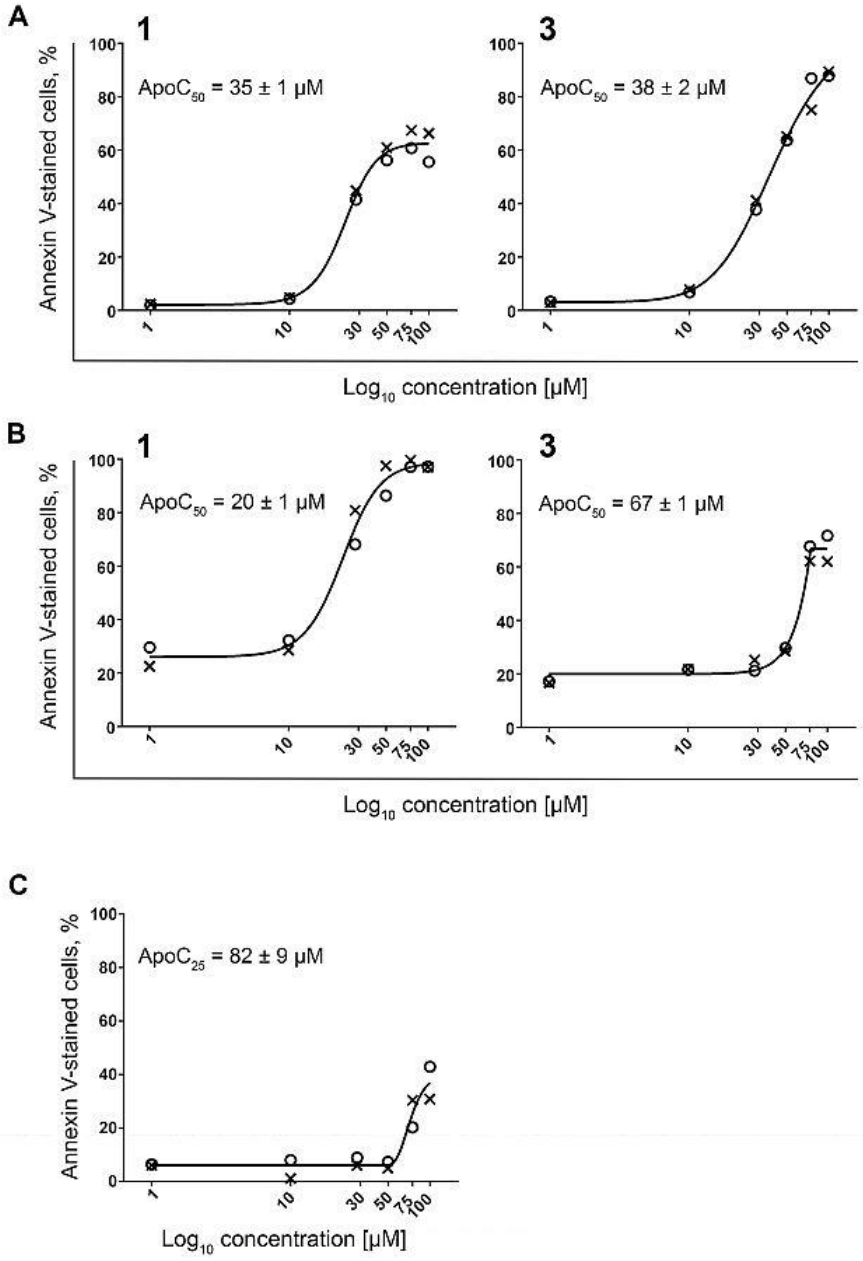

Fig. S11. Concentration-response curves for investigated complexes on THP-1 (A) and MCF-7 (B) cells, and for cisplatin on MCF-7 cell (C). All results are presented as percentages of apoptotic cells determined by means of Annexin V/PI double staining method for two independent experiments (circles and crosses). $ApoC_{50}$ and $ApoC_{25}$ concentrations were computed using asymmetric five-parameter sigmoidal curve in GraphPad Prism software.

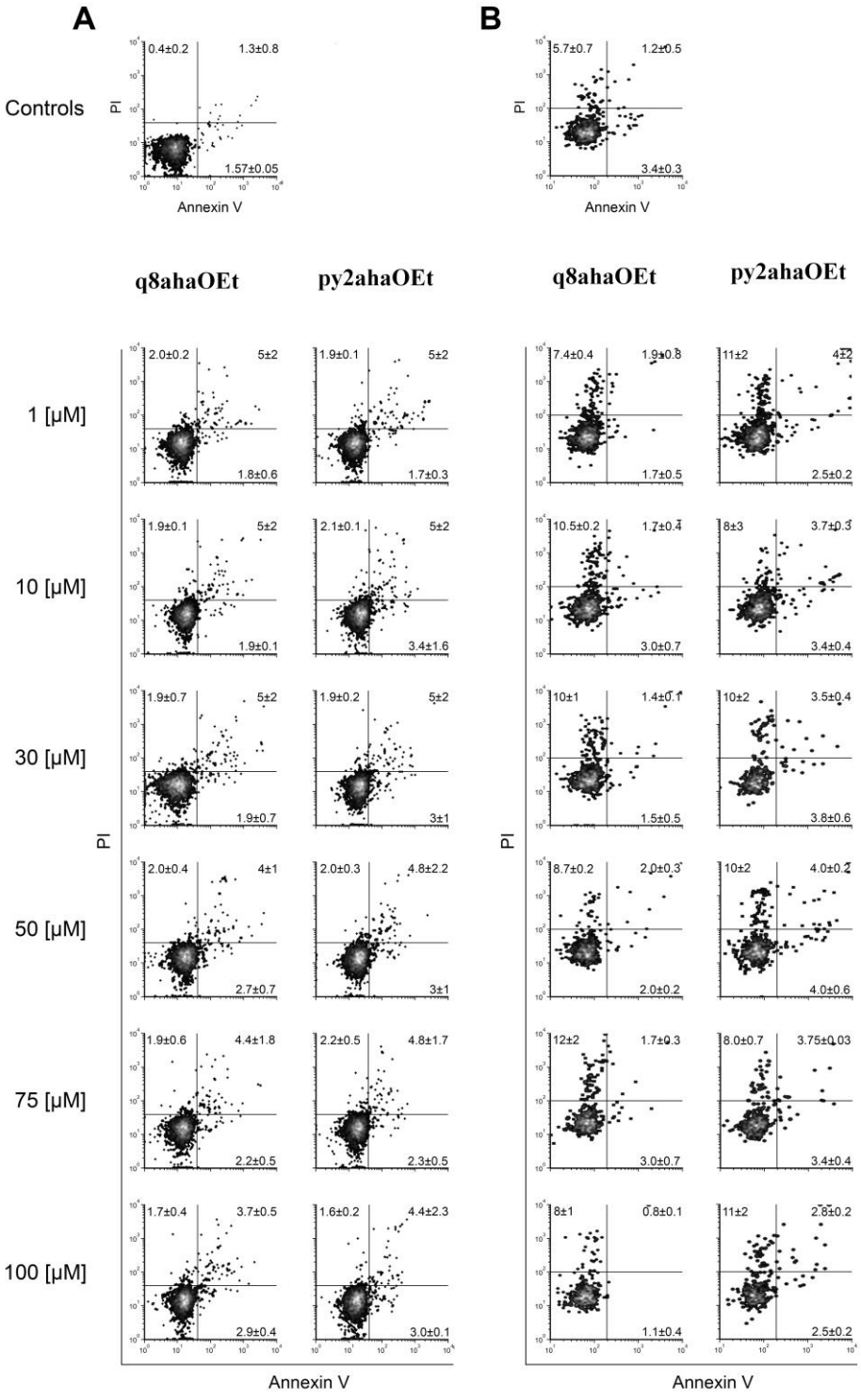

Fig. S12. Different types of cell death in THP-1 (A) and MCF-7 (B) cells treated with investigated compounds. The types were determined by means of Annexin V/PI assay after 24 h incubation. Results are represented as the mean ± SD percentages of two replicates from independent experiments.

Complex 3 challenges independent activation of intrinsic and extrinsic apoptosis pathways in both treated cell lines

To assess the degree of apoptosis dependency on caspase activation, we tested how co-incubation of cells with investigated compound and pancaspase inhibitor Z-VAD-fmk affect mode of cell death compared to samples treated with investigated compound only. For that matter, influence of caspases inhibition on both necrosis and apoptosis was followed, while within apoptotic death early and advanced phases were observed separately. This approach allows reviewing which of those events are impacted in term of inhibition or stimulation due to the lack of caspase activity.

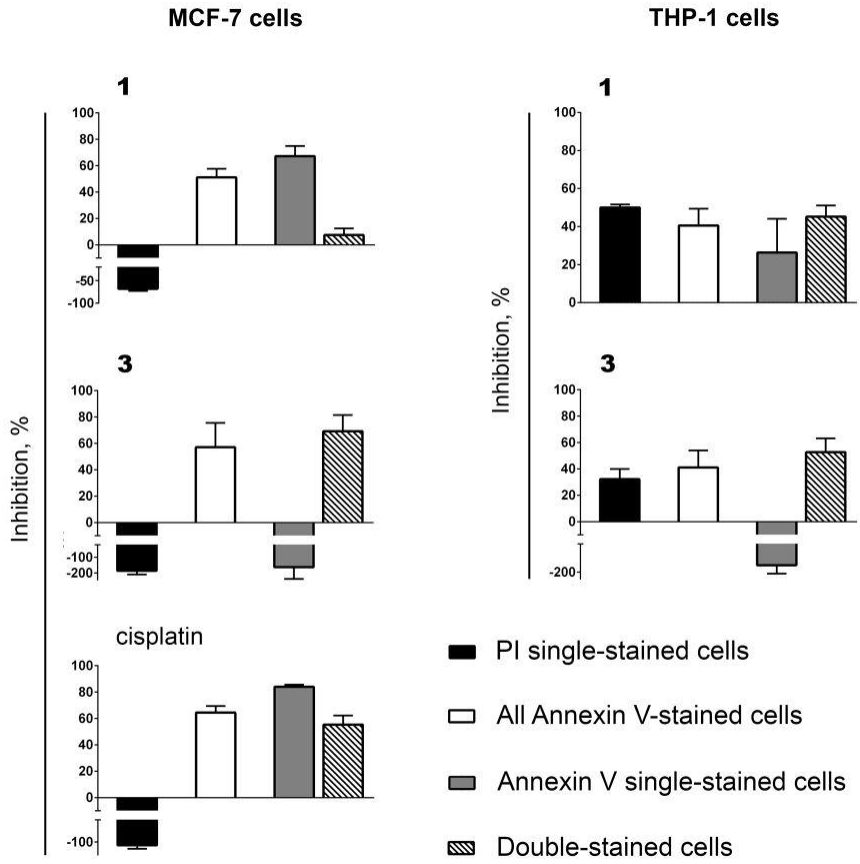

Fig. S13. Percentages of cell death inhibition in cells due to co-incubation with pan-caspase inhibitor carbobenzoxy-valyl-alanyl-aspartyl-[O-methyl]-fluoro methylketone (Z-VAD-fmk) and investigated compounds, determined by means of Annexin V/PI staining method after 6 h of incubation. Results are expressed as the mean ± SD of two replicates from independent experiments.

As it can be seen in Figure S13, inhibition of caspase activity in THP-1 cells results in almost identical percentages of suppressed apoptotic events: 41 ± 9 % and 41 ± 13 % in samples subjected to **1** and **3**, respectively. Necrosis is also inhibited but in a different extent between those treatments (50 ± 2 % and 32 ± 7 % for **1** and **3**, respectively). However, there is significant discrepancy regarding impact of caspase inhibition on early and advanced phases of apoptotic process. There is a significant increase of Annexin V single-stained events in THP-1 cells co-incubated with Z-VAD-fmk and **3** that demonstrates initiation of apoptotic death by this compound is actually caspase-independent (–155 ± 53 %). On the other hand, both early and late phases of apoptosis in **1**-treated THP-1 cells are inhibited.

Likely to results reviewed in THP-1 cells, the addition of Z-VAD-fmk to MCF-7 cells subjected to each of investigated compounds reduces incidence of apoptotic deaths in a similar extent (51 ± 6 % and 57 ± 18 % for **1** and **3**, respectively, Figure S13). Furthermore, caspase-independent initiation of apoptotic death described above in THP-1 samples subjected to **3** here is seen in MCF-7 cells too (–162 ± 74 %), together with strong caspase-dependency of its advanced phases (69 ± 12 %). On the contrary, induction of apoptosis with **1** displays strong caspase-dependency (67 ± 8 %), while its evolution is barely affected by inhibition of caspase cascades (7 ± 4 %).

Although process of necrotic death, either being controlled or accidental, is not directly related to, or managed by activation of caspase pathways, assessment of necrosis feedback to co-incubation with pan-caspase inhibitor may provide additional information. Commonly, it is expected that percentage of necrotic cells increases due to addition of Z-VAD-fmk as a consequence of interrupted apoptotic signaling transduction. However, if in the samples treated with investigated compound majority of necrotic cells result as a downstream events subsequently to triggered apoptosis (aponecrosis) [S25, S26], it can be expected that obstructed inception of apoptosis due to presence of pan-caspase inhibitor might consequently decreases the incidence of necrosis in Z-VAD-fmk co-treated samples. Even that percentage of necrotic cells is negligible in THP-1 samples evaluated after 24 h treatment with either **1** or **3** (Figure 1A, main text), results of the current experiment reveal that aponecrosis can occurs as an early event (Figure S13). On the contrary, necrosis is notably present in some MCF-7 samples after 24 h incubation with investigated compounds (Figure 1B, main text), but addition of Z-VAD-fmk results with meaningful augmentation of necrotic events. Those facts indicate that necrosis in MCF-7 cells subjected to **1** and **3** is most probably developed independently of apoptosis.

Previously, we reviewed that apoptosis in THP-1 cells caused by the treatment with cisplatin was modestly caspase-dependent (23.5 ± 12 % of apoptotic events inhibited by Z-VAD-fmk) [S27]. Here in MCF-7 cells (Figure S13), apoptosis challenged by cisplatin displays strong caspase-dependency (64 ± 5 % of inhibition), particularly its initiation (84 ± 2 %) as well as process of its evolution (55 ± 7 %). There is obvious phenotypically specific response of THP-1 and MCF-7 cells to cisplatin, which is even more pronounced in terms of results on activity of caspase-8 and -9.

Complex 1 achieves superior inhibition of MCF-7 spheroids' growth than other tested compounds

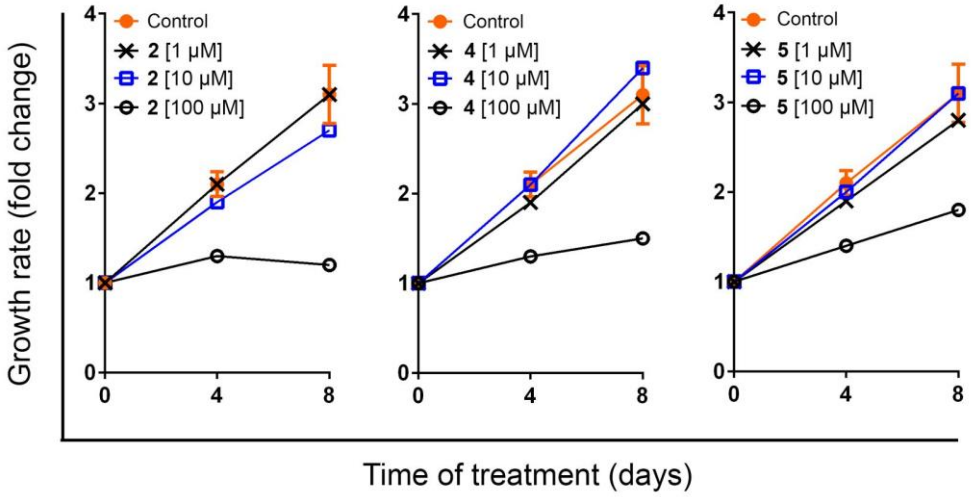

Fig. S14. Growth rate graphs for MCF-7 3D spheroids non-treated and treated with investigated complex. Results are represented as the fold change of a single replicate.

Spectroscopic studies revealed binding of 1 and 3 to human serum albumin (HSA)

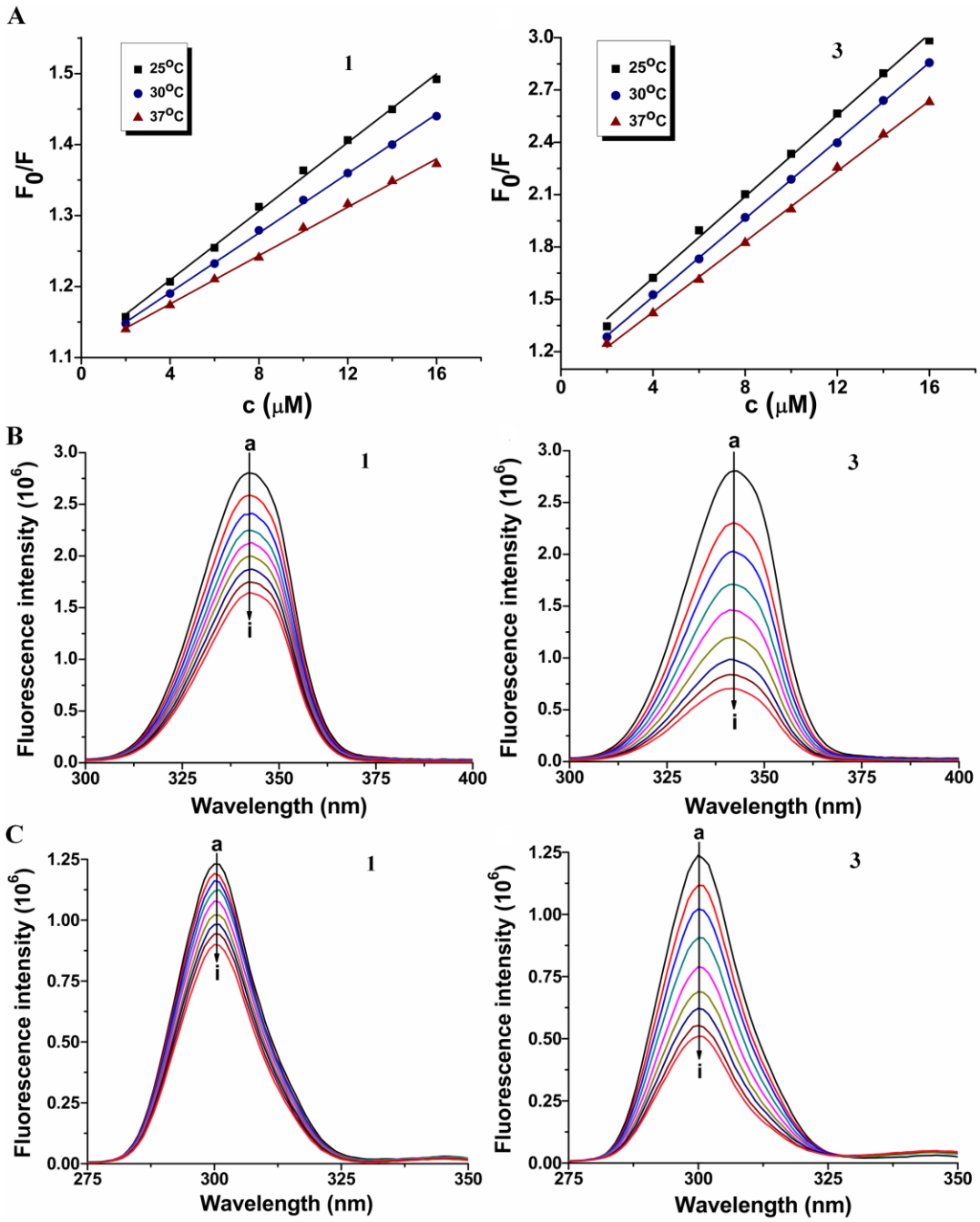

Fig. S15. (A) Stern–Volmer plots of HSA fluorescence quenched by **1** or **3** at three different temperatures. Synchronous fluorescence spectra of HSA (1 μM) with (B) Δλ = 60 nm (Trp) and (C) Δλ = 15 nm (Tyr) in the presence of increasing concentration of Pd-ligands (0-14 μM) for curves a to i, respectively.

Docking of 1 and 3 to Topoisomerases

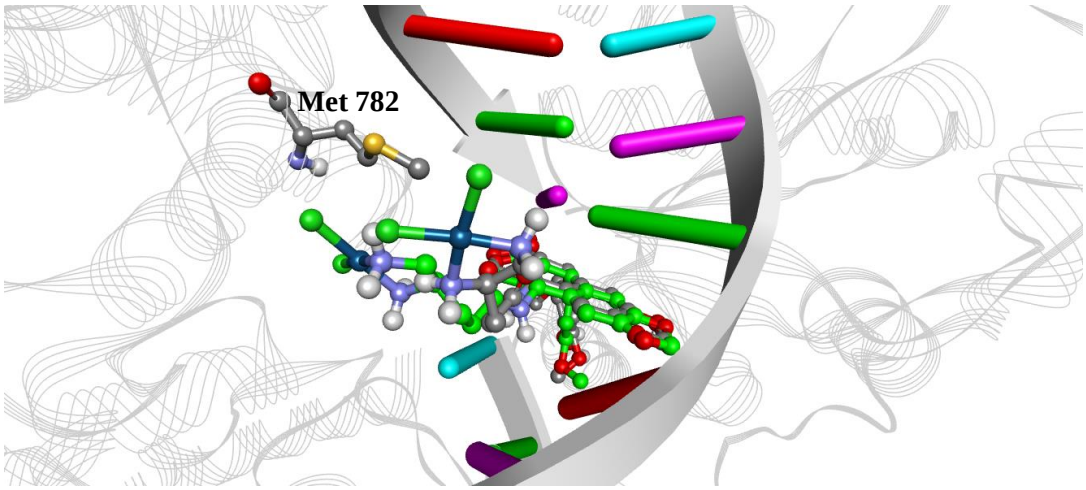

Fig. S16. Etoplatin position from crystal structure 5GWI (green carbon atoms) and docked pose (grey carbon atoms). Met 782 is also presented.

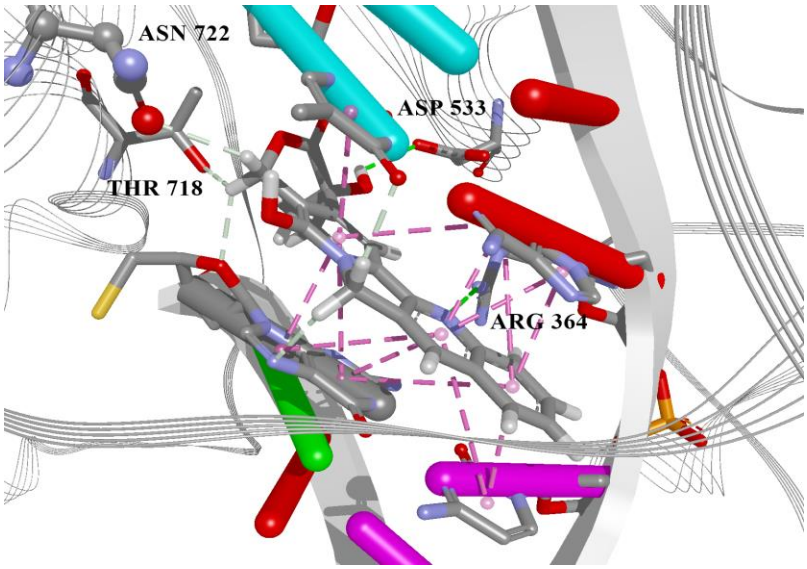

Fig. S17. Crystal coordinates of camptothecin in active site of Top I. Green: hydrophilic interactions. Purple/grey: aromatic and other hydrophobic interactions.

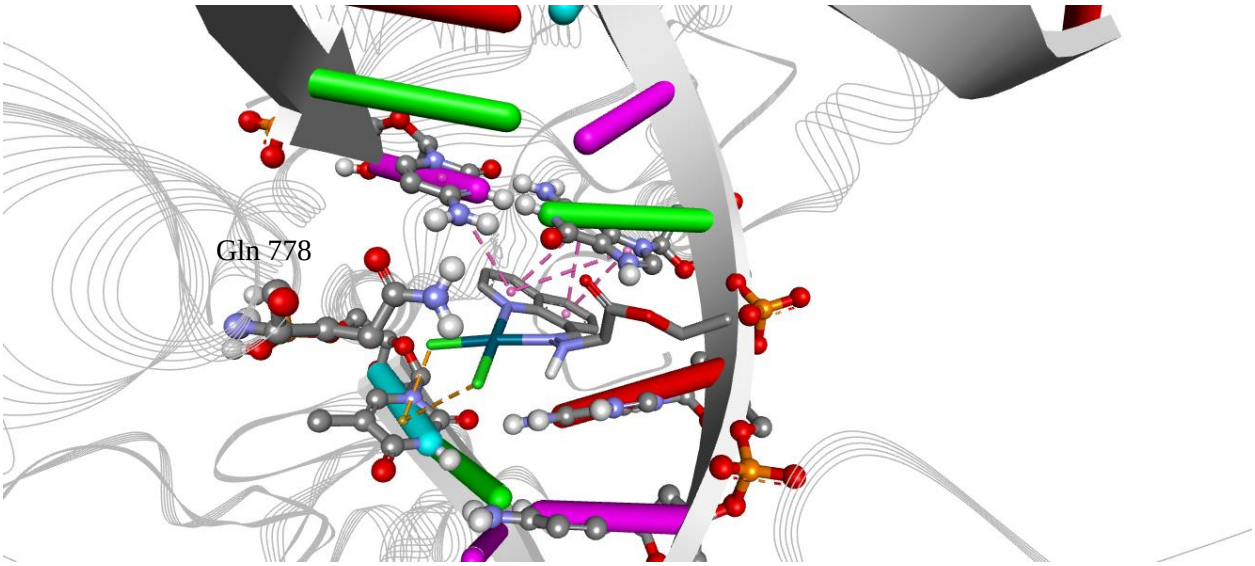

Fig. S18. Compound **1** docked in Top II active site, DNA pocket.

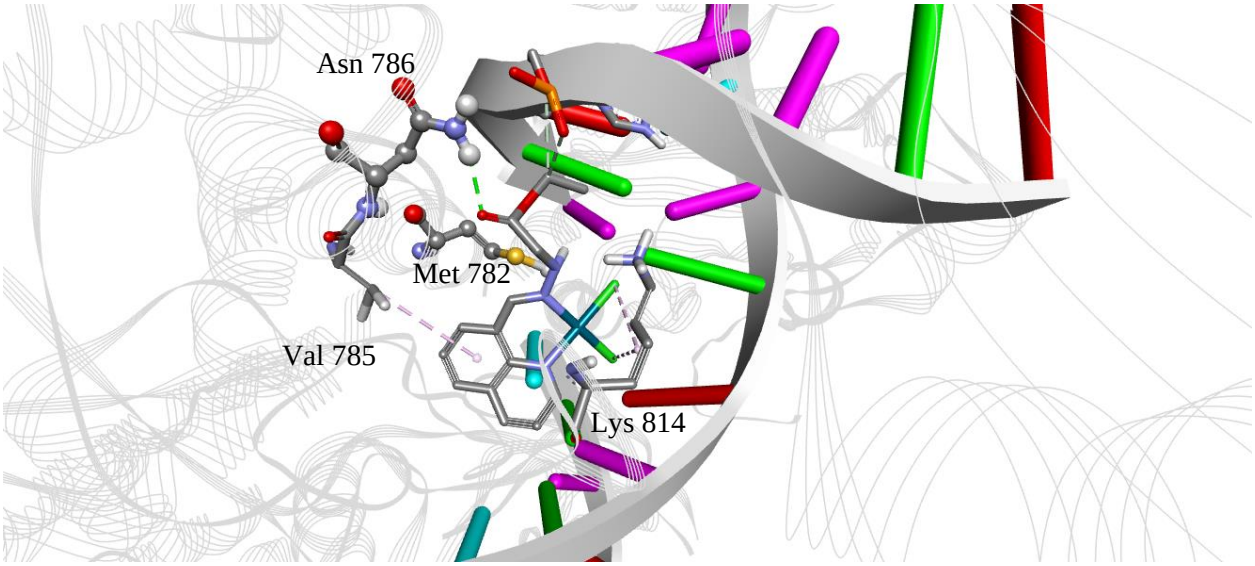

Fig. S19. Compound **1** docked in Top II active site, Met 782 pocket.

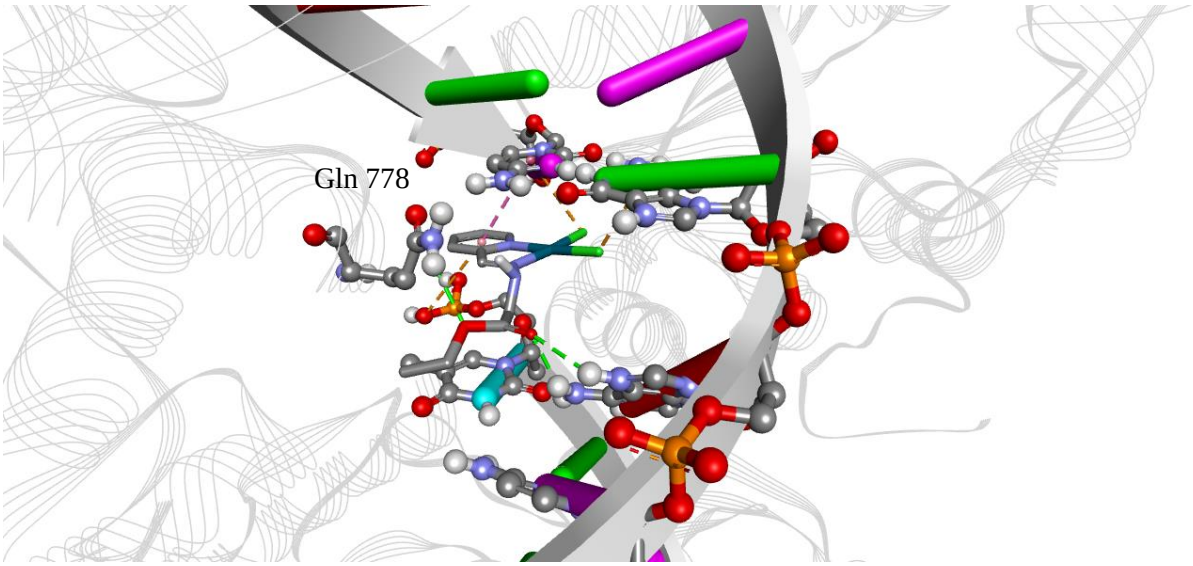

Fig. S20. Compound **3** docked in Top II active site, DNA pocket. Green lines: hydrophilic interactions. Orange/purple: hydrophobic.

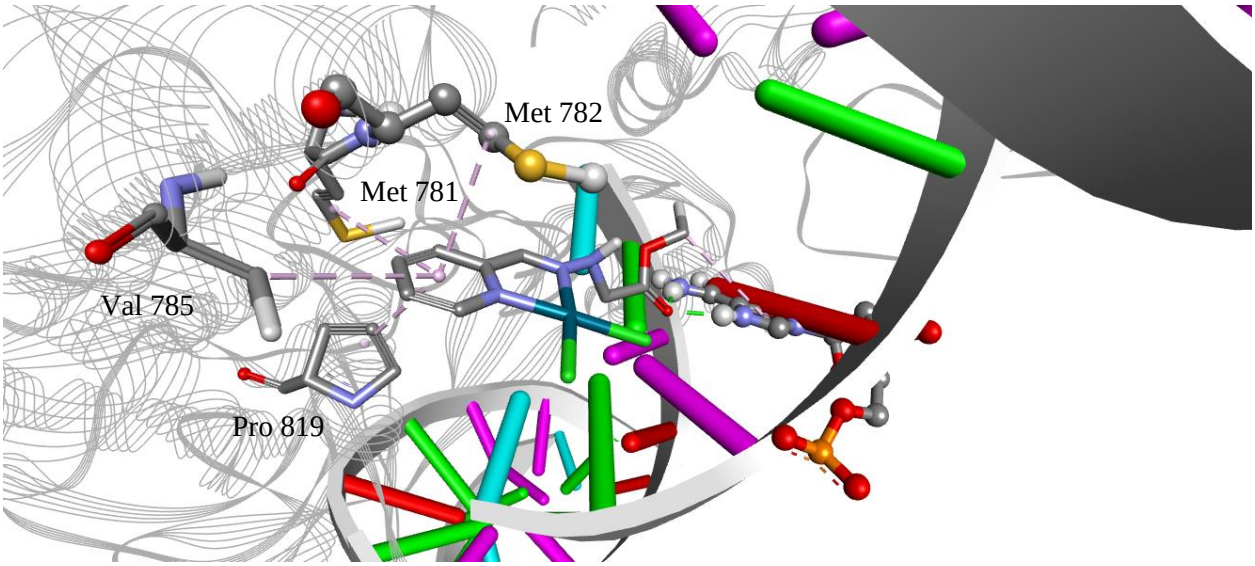

Fig. S21. Compound **3** docked in Top II active site, Met 782 pocket.

DNA Top I Inhibitory Activity of 1 and 3

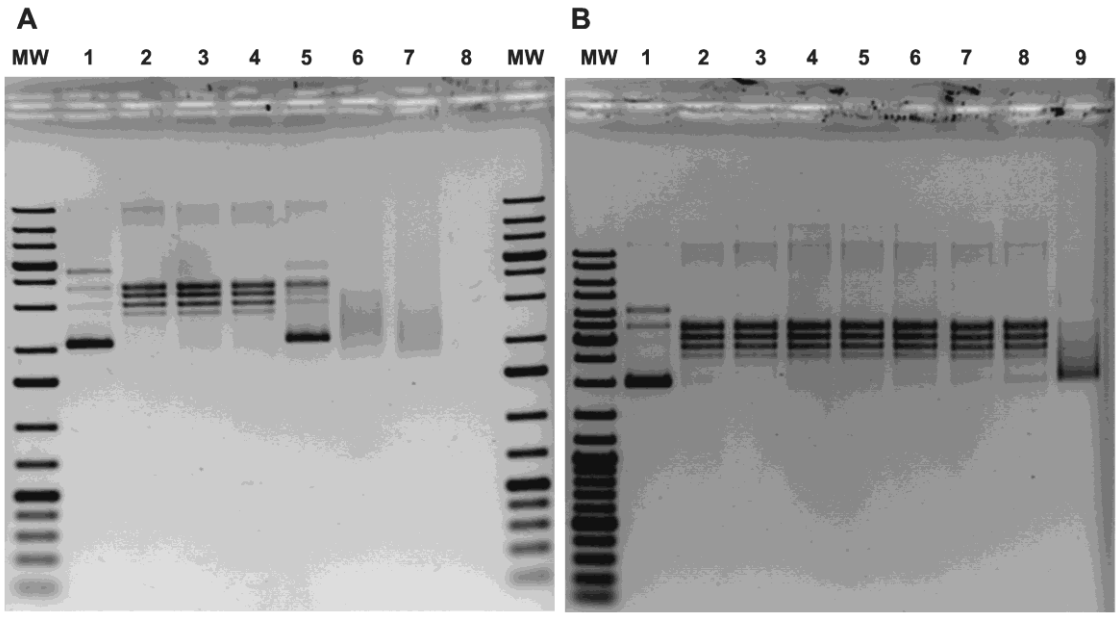

Fig. S22. Agarose gel showing a inhibition of Top I with increasing concentrations of **3**. Lanes: (A - MW) GeneRuler 1 kb Plus DNA Ladder 0.1-20 kb (Thermo Fisher Scientific); (B - MW) GeneRuler DNA LadderMix 0.1-10 kb (Thermo Fisher Scientific); (A and B - 1) pBlueScript SK (-) without Top I; (A and B - 2) pBlueScript SK (-) with Top I; (A 3-8 and B 3-9) pBlueScript SK (-) with Top I and increasing concentrations of 3: (A3) 0.1 µM; (A4) 1 µM; (A5) 10 µM; (A6) 100 µM; (A7) 500 µM; (A8) 1000 µM; (B3) 0.1 µM; (B4) 1 µM; (B5) 2 µM; (B6) 4 µM; (B7) 6 µM; (B8) 8 µM; (B9) 10 µM.

Gel electrophoresis study of interactions of 1 and 3 with plasmid DNA

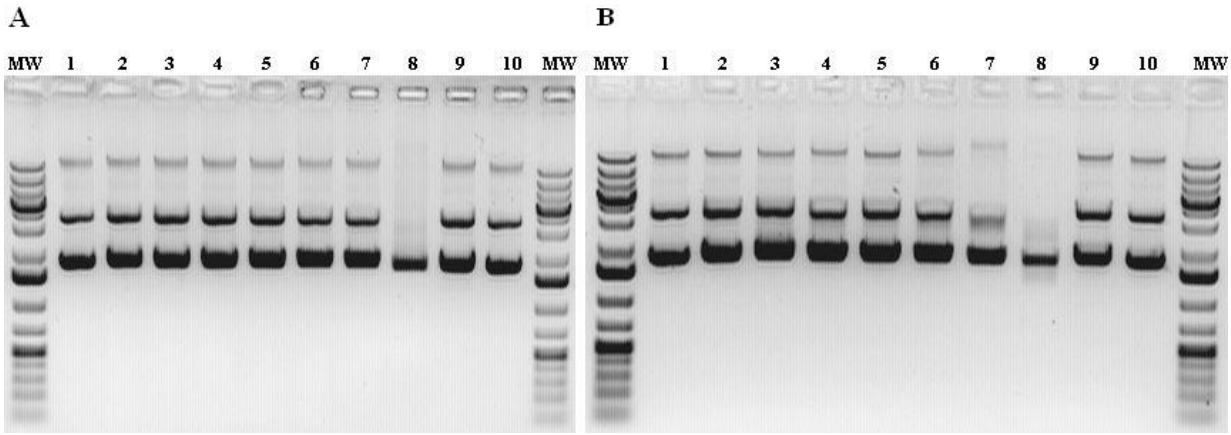

Fig. S23. Results of agarose gel electrophoresis of interaction of pBlueScript SK (-) plasmid with **1** (A) and **3** (B) after 120 minutes of incubation. Lane 1 – control plasmid pBlueScript SK (-); lane 2, 3, 4, 5, 6, 7 and 8 – plasmid pBlueScript SK (-) with 50 μM, 100 μM, 200 μM, 300 μM, 500 μM, 750 μM and 1000 μM of corresponding the complex, respectively; lane 9 – control plasmid pBlueScript SK (-) + 3 μM of DMSO; Lane 10 – control plasmid pBlueScript SK (-); MW - GeneRuler 1 kb Plus DNA Ladder 0.1-20 kb (Thermo Fisher Scientific).

References

[S1] N.R. Filipović, I. Marković, D. Mitić, N. Polović, M. Milčić, M. Dulović, M. Jovanović, M. Savić, M. Nikšić, K. Anđelković, T. Todorović, A Comparative Study of In Vitro Cytotoxic, Antioxidant, and Antimicrobial Activity of Pt(II), Zn(II), Cu(II), and Co(III) Complexes with N -heteroaromatic Schiff Base (*E*)-2-[N′-(1-pyridin-2-yl-ethylidene)hydrazino]acetate, J. Biochem. Mol. Toxicol. 28 (2014) 99–110. doi:10.1002/jbt.21541.

[S2] J.R. Lakowicz, Principles of Fluorescence Spectroscopy, 3rd ed., Springer Science Business Media, New York, USA, 2006, 2006.

[S3] Q.L.S. Lu, T. Cui, Applications of Circular Dichroism and Optical Rotatory Dispersion in Molecular Biology, 1st ed., Science Press, 1987.

[S4] J. Ghuman, P.A. Zunszain, I. Petitpas, A.A. Bhattacharya, M. Otagiri, S. Curry, Structural Basis of the Drug-binding Specificity of Human Serum Albumin, J. Mol. Biol. 353 (2005) 38–52. doi:10.1016/j.jmb.2005.07.075.

[S5] D. Wei, W.D. Wilson, S. Neidle, Small-molecule binding to the DNA minor groove is mediated by a conserved water cluster, J. Am. Chem. Soc. 135 (2013) 1369–1377. doi:10.1021/ja308952y.

[S6] W. Zhu, Y. Wang, K. Li, J. Gao, C.H. Huang, C.C. Chen, T.P. Ko, Y. Zhang, R.T. Guo, E. Oldfield, Antibacterial drug leads: DNA and enzyme multitargeting, J. Med. Chem. 58 (2015) 1215–1227. doi:10.1021/jm501449u.

[S7] B.L. Staker, M.D. Feese, M. Cushman, Y. Pommier, D. Zembower, L. Stewart, A.B. Burgin, Structures of three classes of anticancer agents bound to the human topoisomerase I-DNA covalent complex, J. Med. Chem. 48 (2005) 2336–2345. doi:10.1021/jm049146p.

[S8] Y.R. Wang, S.F. Chen, C.C. Wu, Y.W. Liao, T.S. Lin, K.T. Liu, Y.S. Chen, T.K. Li, T.C. Chien, N.L. Chan, Producing irreversible topoisomerase II-mediated DNA breaks by site-specific Pt(II)-methionine coordination chemistry, Nucleic Acids Res. 45 (2017) 10861–10871. doi:10.1093/nar/gkx742.

[S9] T. a Halgren, Merck Molecular Force Field., J. Comput. Chem. 17 (1996) 490–519. doi:10.1002/(SICI)1096-987X(199604)17:5/6<520::AID-JCC2>3.0.CO;2-W.

[S10] S. Grimme, Semiempirical GGA-type density functional constructed with a long-range dispersion correction., J. Comput. Chem. 27 (2006) 1787–99. doi:10.1002/jcc.20495.

[S11] G.A. Petersson, M.A. Al-Laham, A complete basis set model chemistry. I. The total energies of closed-shell atoms and hydrides of the first-row elements, J. Chem. Phys. 89 (1988) 2193. doi:10.1063/1.460447.

[S12] G.A. Peterson, M.A. Al-Laham, A complete basis set model chemistry. II. Open-shell systems and the total energiesof the first-row atoms, J. Chem. Phys. 94 (1991) 6081–6090.

[S13] P.J. Hay, W.R. Wadt, Ab initio effective core potentials for molecular calculations. Potentials for the transition metal atoms Sc to Hg, J. Chem. Phys. 82 (1985) 270–283. doi:10.1063/1.448799.

[S14] W.R. Wadt, P.J. Hay, Ab initio effective core potentials for molecular calculations. Potentials for main group elements Na to Bi, J. Chem. Phys. 82 (1985) 284–298. doi:10.1063/1.448800.

[S15] P.J. Hay, W.R. Wadt, *Ab initio* effective core potentials for molecular calculations. Potentials for K to Au including the outermost core orbitals, J. Chem. Phys. 82 (1985) 299–310. doi:10.1063/1.448975.

[S16] M. J. Frisch, G. W. Trucks, H. B. Schlegel, G. E. Scuseria, M. A. Robb, J. R. Cheeseman, G. Scalmani, V. Barone, B. Mennucci, G. A. Petersson, H. Nakatsuji, M. Caricato, X. Li, H. P. Hratchian, A. F. Izmaylov, J. Bloino, G. Zheng, J. L. Sonnenberg, M. Hada, M. Ehara, K. Toyota, R. Fukuda, J. Hasegawa, M. Ishida, T. Nakajima, Y. Honda, O. Kitao, H. Nakai, T. Vreven, J. A. Montgomery, Jr., J. E. Peralta, F. Ogliaro, M. Bearpark, J. J. Heyd, E. Brothers, K. N. Kudin, V. N. Staroverov, R. Kobayashi, J. Normand, K. Raghavachari, A. Rendell, J. C. Burant, S. S. Iyengar, J. Tomasi, M. Cossi, N. Rega, J. M. Millam, M. Klene, J. E. Knox, J. B. Cross, V. Bakken, C. Adamo, J. Jaramillo, R. Gomperts, R. E. Stratmann, O. Yazyev, A. J. Austin, R. Cammi, C. Pomelli, J. W. Ochterski, R. L. Martin, K. Morokuma, V. G. Zakrzewski, G. A. Voth, P. Salvador, J. J. Dannenberg, S. Dapprich, A. D. Daniels, Ö. Farkas, J. B. Foresman, J. V. Ortiz, J. Cioslowski, D. J. Fox, Gaussian 09, Revision E.01, (2009).

[S17] M.F. Sanner, Python: a programming language for software integration and development., J. Mol. Graph. Model. 17 (1999) 57–61.

[S18] G.M. Morris, R. Huey, W. Lindstrom, M.F. Sanner, R.K. Belew, D.S. Goodsell, A.J. Olson, AutoDock4 and AutoDockTools4: Automated docking with selective receptor flexibility., J. Comput. Chem. 30 (2009) 2785–91. doi:10.1002/jcc.21256.

[S19] U. James J. P. Stewart, Stewart Computational Chemistry, Colorado Springs, CO, MOPAC 2016, (2016).

[S20] J.J.P. Stewart, Optimization of parameters for semiempirical methods VI: More modifications to the NDDO approximations and re-optimization of parameters, J. Mol. Model. 19 (2013) 1–32. doi:10.1007/s00894-012-1667-x.

[S21] N. Filipović, S. Grubišić, M. Jovanović, M. Dulović, I. Marković, O. Klisurić, A. Marinković, D. Mitić, K. Anđelković, T. Todorović, Palladium(II) Complexes with N-Heteroaromatic Bidentate Hydrazone Ligands: The Effect of the Chelate Ring Size and Lipophilicity on *in vitro* Cytotoxic Activity, Chem. Biol. Drug Des. 84 (2014) 333–341. doi:10.1111/cbdd.12322.

[S22] W.J. Geary, The use of conductivity measurements in organic solvents for the characterisation of coordination compounds, Coord. Chem. Rev. 7 (1971) 81–122. doi:10.1016/S0010-8545(00)80009-0.

[S23] L. Yang, D.R. Powell, R.P. Houser, Structural variation in copper(I) complexes with pyridylmethylamide ligands: structural analysis with a new four-coordinate geometry index, tau4., Dalton Trans. (2007) 955–964. doi:10.1039/b617136b.

[S24] G.A. Jeffrey, H. Maluszynska, J. Mitra, Hydrogen bonding in nucleosides and

nucleotides, Int. J. Biol. Macromol. 7 (1985) 336–348. doi:10.1016/0141-8130(85)90048-0.

[S25] F. Shaki, M.J. Hosseini, M. Ghazi-Khansari, J. Pourahmad, Depleted uranium induces disruption of energy homeostasis and oxidative stress in isolated rat brain mitochondria. Metallomics 5 (2013) 736–744. doi: 10.1039/c3mt00019b.

[S26] G. Gasser G, I. Ott, N. Metzler-Nolte, Organometallic anticancer compounds. J. Med Chem. 54 (2011) 3–25. doi: 10.1021/jm100020w.

[S27] M. Marloye, G. Berger, M. Gelbcke, F. Dufrasne, A survey of the mechanisms of action of anticancer transition metal complexes. Future Med. Chem. 8 (2016) 2263–2286. doi: 10.4155/fmc-2016-0153.